Is spontaneous coronary artery dissection (SCAD) related to local anatomy and hemodynamics? An exploratory study

International Journal of Cardiology 386 (2023) 1–7

Contents lists available at ScienceDirect

International Journal of Cardiology

journal homepage: www.elsevier.com/locate/ijcard

Is spontaneous coronary artery dissection (SCAD) related to local anatomy and hemodynamics? An exploratory study

Alessandro Candreva [a,b], Maurizio Lodi Rizzini [b], Victor Schweiger [a], Diego Gallo [b], Rocco A. Montone [c], Michael Würdinger [a], Julia Stehli [a], Thomas Gilhofer [a], Alexander Gotschy [a], Ruschitzka Frank [a,d], Barbara E. Stähli [a,d], Claudio Chiastra [b], Umberto Morbiducci [b,1], Christian Templin [a,d,*,1]

[a] Department of Cardiology, University Heart Center, Zurich University Hospital, Zurich, Switzerland
[b] PoliTo^{BIO} Med Lab, Department of Mechanical and Aerospace Engineering, Politecnico di Torino, Turin, Italy
[c] Department of Cardiovascular Medicine, Fondazione Policlinico Universitario A. Gemelli IRCCS, Rome, Italy
[d] University of Zurich, Zurich, Switzerland

ARTICLE INFO

Keywords:
Spontaneous coronary artery dissection
Coronary tortuosity
Computational fluid dynamics
Wall shear stress

ABSTRACT

Aims: Spontaneous coronary artery dissection (SCAD) is an increasingly diagnosed cause of myocardial infarction with unclear pathophysiology. The aim of the study was to test if vascular segments site of SCAD present distinctive local anatomy and hemodynamic profiles.

Methods: Coronary arteries with spontaneously healed SCAD (confirmed by follow-up angiography) underwent three-dimensional reconstruction, morphometric analysis with definition of vessel local curvature and torsion, and computational fluid dynamics (CFD) simulations with derivation of time-averaged wall shear stress (TAWSS) and topological shear variation index (TSVI). The (reconstructed) healed proximal SCAD segment was visually inspected for co-localization with curvature, torsion, and CFD-derived quantities hot spots.

Results: Thirteen vessels with healed SCAD underwent the morpho-functional analysis. Median time between baseline and follow-up coronary angiograms was 57 (interquartile range [IQR] 45–95) days. In seven cases (53.8%), SCAD was classified as type 2b and occurred in the left anterior descending artery or near a bifurcation. In all cases (100%), at least one hot spot co-localized within the healed proximal SCAD segment, in 9 cases (69.2%) $\geq$ 3 hot spots were identified. Healed SCAD in proximity of a coronary bifurcation presented lower TAWSS peak values (6.65 [IQR 6.20–13.20] *vs.* 3.81 [2.53–5.17] Pa, $p = 0.008$) and hosted less frequently TSVI hot spots (100% *vs.* 57.1%, $p = 0.034$).

Conclusion: Vascular segments of healed SCAD were characterized by high curvature/torsion and WSS profiles reflecting increased local flow disturbances. Hence, a pathophysiological role of the interaction between vessel anatomy and shear forces in SCAD is hypothesized.

1. Introduction

Spontaneous coronary artery dissection (SCAD) is an emergently recognised clinical condition, leading to acute myocardial infarction (MI), cardiac arrest, and cardiac death in a mostly younger patient population with a higher female prevalence [1,2]. Being angiographically recognised as a luminal narrowing with or without the presence of a radiolucent flap or a false lumen retaining contrast medium [3], pathophysiological mechanics of SCAD still remain unclear. In fact, whereas a spontaneous intimal tear and intramural hematoma are the two recognised main pathophysiological mechanisms of the intimo-medial flap and false lumen generation [4], the underlying biological

Abbreviations: CFD, Computational fluid dynamics; MI, Myocardial infarction; QCA, Quantitative coronary angiography; SCAD, Spontaneous coronary artery dissection; ROI, Region of interest; TAWSS, Time-averaged WSS; TSVI, Topological shear variation index; VMTK, Vascular modeling toolkit; WSS, Wall shear stress.

* Corresponding author at: Andreas Grüntzig Heart Catheterization Laboratory, University Heart Center, University Hospital Zurich, Rämistrasse 100, CH-8091 Zurich, Switzerland.
E-mail address: christian.templin@usz.ch (C. Templin).

[1] Equal contribution.

https://doi.org/10.1016/j.ijcard.2023.05.006
Received 7 March 2023; Received in revised form 16 April 2023; Accepted 5 May 2023
Available online 16 May 2023

events triggering these phenomena remain to be elucidated. Among others, hormonal conditions, systemic inflammatory diseases, and arteriopathies were identified as predisposing conditions for SCAD development [3]. Moreover, it was reported that a tortuous coronary anatomy is highly prevalent in SCAD, pointing towards a role of adverse anatomical features in the mechanisms for arterial dissection [5]. In this regard, as anatomy shapes blood flow [6], the association between SCAD and vascular anatomical features suggests an involvement of local hemodynamic forces in SCAD.

Personalized computational fluid dynamics (CFD) simulations have recently gained scientific momentum as valuable investigational tool of the intracoronary hemodynamics [7,8], allowing the calculation of the wall shear stress (WSS) acting at the level of the endothelium-blood interface. WSS profiles were related to adverse coronary events [9], even in vessels presenting non-flow-limiting lesions [10]. WSS-based quantities have demonstrated to be capable to reflect near-wall flow disturbances, e.g. identifying coronary lesions prone to cause a MI [11].

In the present study, morphometric analysis and personalized CFD simulations were used to investigate local anatomy and hemodynamics at sites of healed SCAD lesions.

2. Methods

2.1. Study population

Consecutive patients with healed SCAD without intracoronary intervention were included in the study. Healed SCADs were defined angiographically as a complete healing of the dissection (‘*restitutio ad integrum*’) at a planned angiographic control (‘second look’) following the first coronary angiogram – when the diagnosis of SCAD was made (‘index procedure’). All included patients provided informed consent and were enrolled retro- or prospectively in the InterSCAD Registry at the University Hospital of Zurich (Zurich, Switzerland).

2.2. SCAD classification and localization

Coronary angiographies were visually assessed by trained personnel (MW, TG and CT). The type of SCAD was adjudicated on the index angiography as per current international consensus [3]. Next, the SCAD proximal initiation point was visually identified at the baseline angiography and localized on the healed vessel segment at the angiographic second look.

2.3. Three-dimensional vessel reconstruction and morphometry assessment

Three-dimensional (3D) quantitative coronary angiography (QCA) reconstructions including bifurcations with side branch diameter larger than 1 mm were performed using two angiographic end-diastolic frames at least 25° apart, combining the QAngio XA Bifurcation RE software (Medis medical imaging systems, Leiden, The Netherlands) and a custom-made algorithm [12]. The vessel centerline, which represents the main geometric attribute of the vessel, was reconstructed using the vascular modeling toolkit (VMTK, Orobix, Bergamo, Italy). Then, a centerline-based morphometric analysis of coronary arteries was performed, with local vessel curvature and torsion values [13] obtained from the reconstructed 3D vessel centerline according to previous studies [14–16]. Briefly, considering a point on a curve in a 3D space (in our case, the vessel centerline), curvature measures how quickly the vessel curves, while torsion measures how quick the vessel twists. Curvature and torsion mathematical definitions are reported in the Supplementary Material.

2.4. Angiography-based blood flow simulations

On the same 3D vessels reconstructions transient CFD simulations were performed adopting the finite volume-based code Fluent (Ansys Inc., Canonsburg, PA, USA). Details on the adopted CFD schemes are reported in the Supplementary Material.

From simulated data, the luminal surface distribution of the time-averaged WSS (TAWSS) and of the topological shear variation index (TSVI) were calculated as in previous studies [7,17]. Briefly, TAWSS represents the value of the WSS magnitude applied to the luminal surface averaged along the cardiac cycle. TSVI quantifies the variability of the contraction/expansion action exerted by the WSS on the endothelium along the cardiac cycle [17,18]. The mathematical formulations of TAWSS and TSVI are reported in the Supplementary Material.

2.5. Anatomical and hemodynamic hot spots assessment and co-localization scoring

Hot spots of curvature and torsion were identified as those local peak values along the centerline belonging to the 90^{th} and 98^{th} percentile, respectively, of the corresponding vessel-specific quantity distribution (Supplementary Fig. 1). A higher percentile (98^{th}) was assumed for torsion given its typical peaked distribution along arterial centerlines. Hot spots of TAWSS and TSVI were identified in terms of luminal surface areas exposed to values belonging to the 90^{th} percentile of the corresponding vessel-specific quantity distribution. Vessel segments and luminal surface areas exposed to peak values were visually mapped on the reconstructed 3D vessels geometry as red areas.

The region of interest (ROI) spanned not beyond 3 mm upstream and downstream from the SCAD proximal initiation point localized on the reconstructed vessel luminal surface: in case a morphometric- or WSS-based quantity hot spot fell within such segments as per visual assessment by three independent observers (AC, MLR and UM), positive co-localization of the given quantity hot spot with the proximal SCAD region was adjudicated with a tick mark (‘V’), see Fig. 1. Conversely, a missing co-localization of a given quantity peak with the ROI was marked with an ‘X’. A co-localization scoring system was implemented and based on the sum of positive co-localization ‘V’ marks, hence ranging from 0 (i.e., absence of hot spots in the ROI) to 4 (i.e., co-localization of all hot spots, of curvature, torsion, TAWSS and TSVI, with the identified segment around SCAD initiation).

2.6. Statistical methods

Statistical analyses were performed on a per-patient and -vessel basis. Bifurcation involvement was used for group-wise comparison. Continuous variables with normal distribution are presented as mean ± standard deviation (SD) and non-normally distributed variables as median (inter-quartile range [IQR]). Categorical variables are presented as percentages. Chi-squared test was used for comparing categorical variables, while Student’s tests or Mann-Whitney tests as appropriate for continuous ones. A p-value <0.05 was considered significant. All analyses were performed using R statistical software (R Foundation for Statistical Computing, Vienna, Austria).

3. Results

From January 1997 to December 2021, 146 patients with angiographically-confirmed SCAD were screened for study inclusion criteria. A spontaneous and complete healing of the SCAD was angiographically documented in 20 subjects (13.7%). Coronary angiography recordings satisfied the criteria for CFD simulations in 13 cases (8.9%), Fig. 2. The angiographic follow-up was performed at 57 (IQR 45–95) days.

3.1. Baseline characteristics

Thirteen patients with thirteen SCAD lesions were included in the analysis. In all but one case (92.3%) an acute trigger at the index event

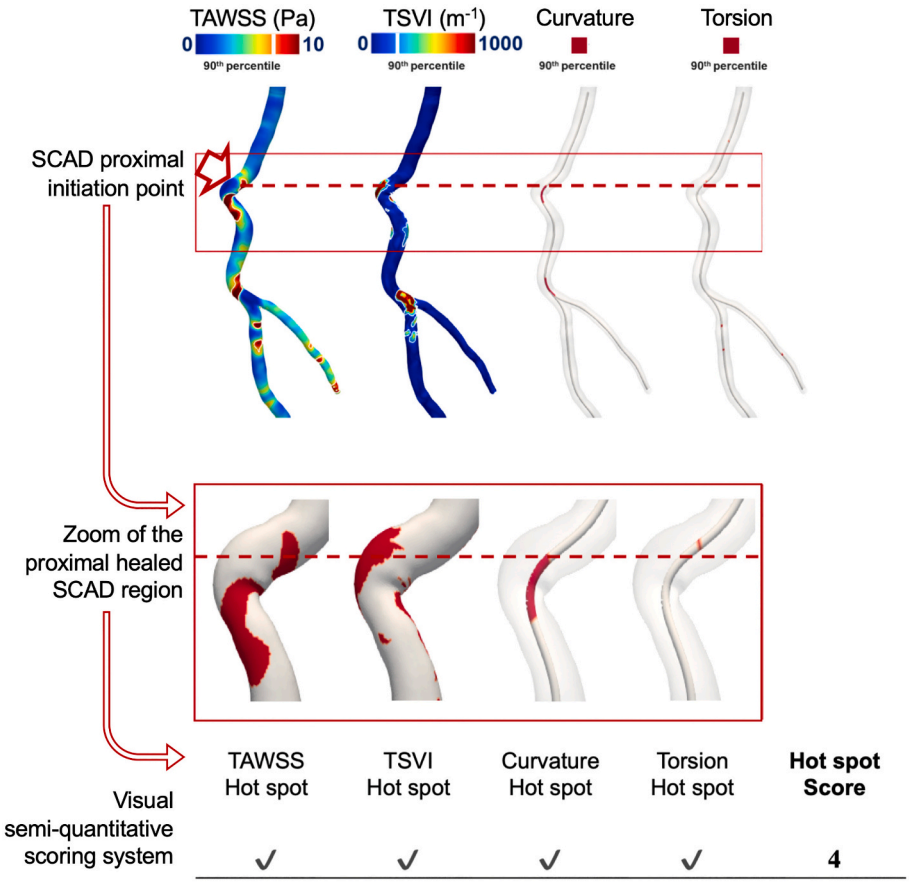

Fig. 1. Case example of co-localization of the hot spots of the four tested variables. Upper panel: The coronary artery with spontaneously healed dissection is reconstructed from the projections from the angiographic second look and the localization of the proximal SCAD initiation point (arrow and dashed line) is obtained from the index angiography. Time-averaged wall shear stress (TAWSS) and topological shear variation index (TSVI) distribution are represented on the vessel luminal reconstruction in a color-coded fashion, while peak values of the curvature and torsion indices are represented in red on the vessel centerlines. Lower panel: Zoom of the proximal region of the healed coronary dissection. TAWSS and TSVI peaks are presented as red stains on the reconstructed vessel luminal surface. The co-localization of the hot spots of the morphometric and WSS-based quantities under investigation is assessed visually. The amount of hot spots co-localizing in the proximity of the proximal SCAD initiation point is obtained and summed up to give the result of the hot spot score (in this case 4). (For interpretation of the references to color in this figure legend, the reader is referred to the web version of this article.)

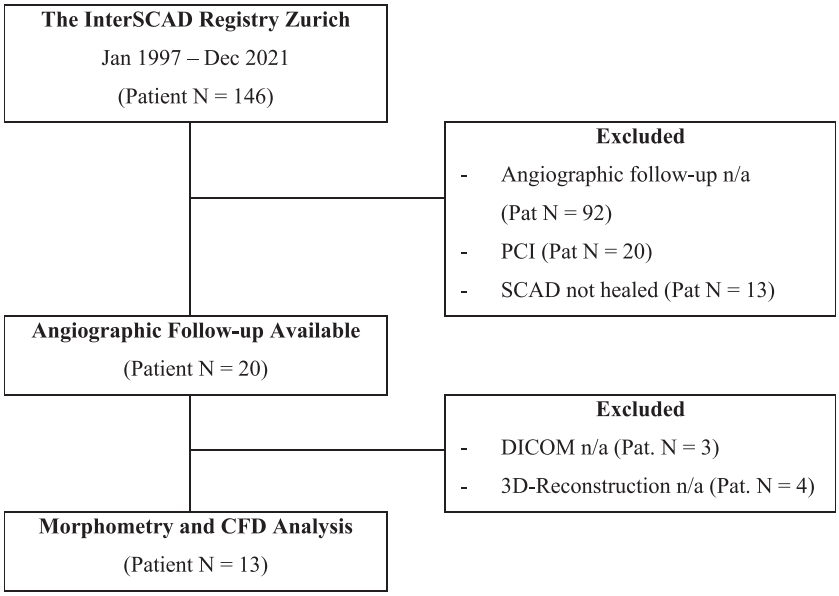

Fig. 2. Study flow chart. Patients were consecutive enrolled in one Swiss tertiary center. Morphometry and computational fluid dynamics (CFD) analysis were performed on those presenting a healed spontaneous coronary dissection (SCAD) with available coronary angiography at the follow-up. In four cases three-dimensional (3D) reconstruction was not possible (in 2 cases the SCAD was located in a side branch with ≤1 mm vessel diameter; in 1 case because of excess in vessel tortuosity; in 1 case for absence of two projections 25° apart with minimal lesion foreshortening).

could be identified, Table 1. Mean age was 46 (IQR 42–62) years, and 10 (76.9%) patients were women. SCAD presented in most cases as non-ST segment elevation myocardial infarction (NSTEMI, 61.5%). Angiographically, type 2b was the most prevalent SCAD variant (53.8%). Baseline parameters were well balanced among patients with healed SCAD regions with and without proximity to a coronary bifurcation, Table 1.

3.2. Anatomical and hemodynamic hot spots co-localization and scoring system

Hot spot adjudication is presented in Fig. 3. From the analysis of the co-localization of the morphometry and WSS hot spots with the SCAD initiation segment emerged that 69.2% of the ROI hosted ≥ 3 hot spots. SCAD ROIs scored on average 2.84 (± 0.66) hot spots and did not differ

Table 1
Baseline characteristics of patients with SCAD with and without proximity to a bifurcation.

	Total SCAD (Patient or Vessel $N = 13$)	SCAD w/o Bifurcation (Patient or Vessel $N = 6$)	SCAD with Bifurcation (Patient or Vessel $N = 7$)	p-value (two-sided)
Age, yrs	46 (42–62)	44 (42–65)	47 (38–62)	0.886
Female gender, n (%)	10 (76.9%)	6 (100.0%)	4 (57.1%)	0.067
BMI, Kg/m^2	27.3 ± 6.73	23.4 ± 4.01	30.7 ± 6.97	0.369
LVEF, %	55.1 ± 6.34	50.8 ± 5.34	58.7 ± 4.82	0.306
Serum creatinine, μmol/L	66.2 ± 13.8	62.7 ± 9.11	69.3 ± 17.0	0.358
Type of ACS:				
- NSTEMI, n (%)	8 (61.5%)	3 (50.0%)	5 (71.4%)	0.429
- STEMI, n (%)	5 (38.5%)	3 (50.0%)	2 (28.6%)	
Type of SCAD:				
- Type 1, n (%)	1 (7.7%)	0 (0.0%)	1 (14.3%)	
- Type 2a, n (%)	5 (38.5%)	3 (50.0%)	2 (28.6%)	0.529
- Type 2b, n (%)	7 (53.8%)	3 (50.0%)	4 (57.1%)	
Type of Vessel:				
- LAD, n (%)	7 (53.8%)	2 (33.3%)	5 (71.4%)	
- LCX, n (%)	5 (38.5%)	4 (66.7%)	1 (14.3%)	0.133
- RCA, n (%)	1 (7.7%)	0 (0.0%)	1 (14.3%)	
Coronary artery disease, n (%)	0 (0.0%)	–	–	
Dilatative arteriopathy, n (%)	4 (30.8%)	1 (16.7%)	3 (42.9%)	0.308
Fibromuscular dysplasia, n (%)	0 (0.0%)	–	–	
Systemic inflammatory disease, n (%)	1 (7.7%)	1 (16.7%)	0 (0.0%)	0.261
Connective tissue disorder, n (%)	0 (0.0%)	–	–	
Hyperthyroidism, n (%)	1 (7.7%)	1 (16.7%)	0 (0.0%)	0.261
Hypertension, n (%)	5 (38.5%)	1 (16.7%)	4 (57.1%)	0.135
T2DM, n (%)	0 (0.0%)	–	–	
Active smoking, n (%)	4 (30.8%)	1 (16.7%)	3 (42.9%)	0.296
Dyslipidemia, n (%)	6 (46.2%)	1 (16.7%)	5 (71.4%)	0.048
ACE-Inhibitor, n (%)	2 (15.4%)	1 (16.7%)	1 (14.3%)	0.906
Aspirin, n (%)	2 (15.4%)	0 (0.0%)	2 (28.6%)	0.155
Oral anticoagulation, n (%)	1 (7.7%)	1 (16.7%)	0 (0.0%)	0.261
Statin, n (%)	2 (15.4%)	1 (16.7%)	1 (14.3%)	0.906
Oral Antidiabetics or Insulin, n (%)	0 (0.0%)	–	–	
Hormonal replacement therapy, n (%)	0 (0.0%)	–	–	
Betablocker, n (%)	0 (0.0%)	–	–	
Calcium-Antagonist, n (%)	0 (0.0%)	–	–	

BMI = Body mass index; LAD = Left anterior descending coronary artery; LCX = Left circumflex coronary artery; LVEF = Left ventricular ejection fraction; NSTEMI = Non-ST elevation myocardial infarction; RCA = Right coronary artery; SCAD = Spontaneous coronary artery dissection; STEMI = ST elevation myocardial infarction; T2DM = Type-2 diabetes mellitus.

between lesions with and without proximity to coronary bifurcations (2.86 ± 0.69 *vs.* 2.83 ± 0.75, $p = 0.954$), Table 2.

3.3. Morphometry in healed SCAD proximal segments

In 12 (92.3%) vessels, anatomical hot spots co-localized with the SCAD offset region. Curvature peaks were more prevalent in healed SCAD regions (84.6%) than torsion peaks (61.5%). The location of curvature and torsion hot spots was not affected by the proximity to a coronary bifurcation (85.7 *vs.* 83.3%, $p = 0.906$ for curvature hot spot with and without proximity to a coronary bifurcation, and 71.4 *vs.* 50.0%, $p = 0.429$ for torsion hot spot in ROI, respectively), Table 2.

3.4. Wall shear stress profiles in healed SCAD proximal segments

In all cases, hot spots of TAWSS and/or TSVI co-localized with the dissection ROI. Both TAWSS and TSVI 90th percentile surface area peak values in the ROI were quantitively higher in the subgroup where the SCAD was not in proximity to a coronary bifurcation (for TAWSS: 3.81 Pa (IQR 2.53–5.17 Pa) *vs.* 6.65 Pa (IQR 6.20–13.20 Pa), $p = 0.008$; for TSVI: 92.60 m^{-1}(IQR 74.04–109.05 m-^{1}] *vs.* 128.98 m^{-1} (IQR 108.44–184.06 m^{-1}), $p = 0.138$). TSVI hot spots site of SCAD were less frequently found in proximity to coronary bifurcations than TAWSS (57.1% *vs.* 100.0%, $p = 0.034$), Table 2.

4. Discussion

The present exploratory study highlighted that vessel segments in the proximal parts of a healed SCAD region were characterized by (i) the presence of local hot spots of curvature and/or torsion as well as of TAWSS and/or TSVI; (ii) the increased prevalence of curvature rather than torsion peaks; and (iii) the presence of local flow disturbances, quantified by WSS.

4.1. Role of coronary anatomy in SCAD pathophysiology

SCAD has traditionally been associated with abnormal vessel geometry, and particularly with tortuosity [3]. Commonly seen in routine angiographies, especially of elderly female patients with long-lasting arterial hypertension [19], coronary tortuosity remains a clinical etiology of unclear definition and clinical significance. It has been experimentally associated with structural changes within the arterial wall (e.g. elastin degradation or deficiency) [20], kinking, and looping arguably originated by an unbalance between tractional, re-tractional, and intraluminal forces applied to the vessel wall, leading ultimately to an irreversible elongation of the vessel [21]. Tortuosity was associated with delayed coronary perfusion [22], and myocardial ischemia in absence of a severe atherosclerotic lesion [23].

Translating long-established notions from the cerebrovascular system to the coronary tree [24], Eleid et al. proposed an analysis with semi-quantitative tortuosity metrics in SCAD based on the visual assessment of the coronary angiogram, which confirmed a strong association between coronary tortuosity and the presence or even the recurrence of SCAD [5]. The same methodology was more recently applied to vessel multiplanar reconstructions from coronary computed tomography angiographies (CCTA), confirming once again an association of coronary tortuosity and SCAD [25]. Conversely, in the present investigation, a vessel centerline-based quantitative analysis performed on 3D vascular geometries reconstructed from coronary angiography was performed [13]. This approach allowed to determine the local curvature and torsion values at any given position along the vessel centerline, identifying in a mathematical manner areas of curvature and/or torsion peaks and consequently allowing to quantify rigorously vessel tortuosity. This made the morphometric analysis automatic, quantitative, and operator independent.

4.2. Role of local hemodynamics in SCAD pathophysiology

Investigations on intracoronary blood flow in the context of SCAD are scarce. This is surprising, given the above discussed link between arterial tortuosity and SCAD, and the well-known impact of arterial anatomy in shaping local hemodynamics [7]. In fact, the presence of sharp bends and non-planarity produces flow separation and stagnation as well as secondary flows and flow recirculation, which in turn may distill into deranged shear force patterns acting on the vessel wall [22]. Among the CFD studies focusing on the hemodynamics in SCAD vessels, Di Donna et al. investigated the role of bifurcations upstream of a dissected coronary segment, identifying that an angle between the left anterior descending coronary artery (LAD) and the first adjacent branch

ANATOMIC-FUNCTIONAL ANALYSIS OF THE PROXIMAL SCAD REGION					
Patient	TAWSS Hot spot	TSVI Hot spot	Curvature Hot spot	Torsion Hot spot	**Hot spot Score**
1	✓	✓	✓	✓	**4**
2	✓	✓	✓	✕	**3**
3	✓	✕	✓	✓	**3**
4	✕	✓	✓	✓	**3**
5	✓	✓	✓	✓	**3**
6	✕	✓	✓	✕	**2**
7	✕	✓	✕	✓	**2**
8	✓	✕	✓	✕	**2**
9	✓	✓	✓	✕	**3**
10	✓	✕	✓	✓	**3**
11	✓	✓	✕	✕	**2**
12	✓	✓	✓	✓	**4**
13	✓	✓	✓	✕	**3**

Fig. 3. Co-localization of morphometric and WSS hot spots with SCAD region. Results of the visual assessment of the co-localization of variable hot spots and proximal dissection area (region of interest or ROI). A match is marked with a tick mark ('V'), a missing match with an 'X'. The count of matches 'V' give the resulting hot spot score for the given vessel. TAWSS = Time-averaged wall shear stress; TSVI = Topological shear variation index.

$< 90°$ can be a cause of increased instantaneous WSS (with diastolic peaks > 2.66 Pa) on the downstream vessel wall, especially in the primary location of the dissection [25]. Here, we found that the cardiac cycle-averaged WSS magnitude (i.e., TAWSS) with median peak > 5.00 Pa co-localized in each analyzed vessel with the proximal dissection end. This evidence could suggest a direct mechanical effect of shear forces on the local endothelium, possibly leading to an intimal tear with increased wall permeability, smoot muscle cell stimulation and elastin degradation [26]. Notably, the mechanism initiated by high WSS action mechanism reconciliates with both theories on the inception of a SCAD, i.e. originating from an endothelial tearing event ('inside-out') or from a vasa vasorum hemorrhage within a elastin-depleted media layer ('outside-in') [3].

In this study, coronary hemodynamics was also quantified by TSVI, a topological skeleton feature of the WSS recently associated with early atherosclerotic changes in coronary arteries and risk of plaque destabilization [11,27]. TSVI was found markedly elevated especially in dissected coronary segments not in proximity of a bifurcation, suggesting a relevance of the complex blood-endothelium interaction pattern captured by this quantity. In fact, TSVI quantifies the variability in the contraction/expansion action exerted by the WSS on the endothelium along the cardiac cycle [17,18]. Recent studies suggested a role for TSVI in altering intracellular and cell-cell tensions [27]. The findings of the study also suggested that the two different mechanisms quantified by TAWSS and TSVI might act separately, but that also might concur to determine the dissection.

4.3. Interaction between vessel geometry and local hemodynamics

The frequent co-localization of hot spots within the ROI might point towards an involvement of the tested anatomic-functional variables in SCAD pathophysiology. A hint might be found when considering the presence or not of coronary bifurcation at the starting point of the dissection. In fact, in these cases numerically higher values for the four tested variables were reported, suggesting that more extreme geometrical and hemodynamic conditions might be necessary in the event of a SCAD in the absence of a vessel partition. Conversely, in the presence of a bifurcation, milder curvatures, torsions, and even less intense shear forces might suffice to favor the offset of a coronary dissection.

In conclusion, a practical implication derived from our data suggests that when SCAD is clinically suspected, a quantitative analysis of the anatomy of the vessel and of the WSS profiles could support the identification of sites prone to dissection propagation/rupture or even re-dissection. In this regard, attention should be focused on areas downstream of bifurcations (particularly towards the daughter branch with a larger deviation angle) and on non-partitioning coronary segments

Table 2
Morphometry and CFD descriptors of healed SCAD lesions with and without proximity to a bifurcation.

		Total SCAD (Vessel N = 13)	SCAD w/o Bifurcation (Vessel N = 6)	SCAD with Bifurcation (Vessel N = 7)	p-value (two-sided)
Morphometry 'hot spot' in ROI, n (%)		12 (92.3%)	6 (100.0%)	6 (85.7%)	1.000
- Curvature Peak Value, mm^{-1}		0.18 0.16–0.29	0.23 0.18–0.32	0.16 0.14–0.29	0.445
- Curvature 'hot spot' in ROI, n (%)		11 (84.6%)	5 (83.3%)	6 (85.7%)	0.906
- Torsion Peak ValueValue, mm^{-1}		2.34 1.97–2.52	2.46 2.34–2.79	2.06 1.49–2.39	0.073
- Torsion 'hot spot' in ROI, n (%)		8 (61.5%)	3 (50.0%)	5 (71.4%)	0.429
CFD 'hot spot' in ROI, n (%)		13 (100.0%)	6 (100.0%)	7 (100.0%)	1.000
- TAWSS Peak Value, Pa		5.17 3.81–6.33	6.65 6.20–13.20	3.81 2.53–5.17	0.008
- TAWSS 'hot spot' in ROI, n (%)		10 (76.9%)	4 (66.7%)	6 (85.7%)	0.416
- TSVI Peak Value, m^{-1}		108.44 74.17–137.74	128.980 108.44–184.06	92.60 74.04–109.05	0.138
- TSVI 'hot spot' in ROI, n (%)		10 (76.9%)	6 (100.0%)	4 (57.1%)	0.034
'Hot spot' SCORE, n (%)	0	0 (0.0%)	0 (0.0%)	0 (0.0%)	
	1	0 (0.0%)	0 (0.0%)	0 (0.0%)	
	2	4 (30.8%)	2 (33.3%)	2 (28.6%)	0.937
	3	7 (53.8%)	3 (50.0%)	4 (57.1%)	
	4	2 (15.4%)	1 (16.7%)	1 (14.3%)	
	Average	2.84 ± 0.66	2.83 ± 0.75	2.86 ± 0.69	0.954

The 'Hot spot' score represents the sum of the 'hot spots' of different morphometry and CFD quantity present within the same ROI. For example, a score equal to two means that two different 'hot spots' (e.g. one of Curvature and one of TSVI) co-localize within the same ROI. CFD = Computational fluid dynamics; ROI = Region of interest; TAWSS = Time-averaged wall shear stress; TSVI = Topological shear variation index.

exhibiting extreme or sequential curvatures and torsions.

4.4. Limitations

This study faces some limitations. First, the number of patients included in the final analysis is relatively small. While explained by selection criteria of the retrospective screening, selection biases cannot be excluded. Second, the underlying study assumptions might not be generalizable. However, evidence exists for a post-SCAD complete healing with *restitutio ad integrum* [1] and orthograde propagation of the dissection was confirmed in the vast majority of cases [28]. Third, the uncertainty and the level of idealization inherent in 3D reconstruction and CFD simulations might have influenced the quantitative anatomical analysis as well as the calculation of WSS-based quantities [29]. Last, no information on vessel thickness and composition (e.g., presence of atherosclerotic process and of vasa vasorum) was available, as intravascular imaging was not routinely performed in these patients. Hence, the influence of these variables on vessel wall tension and the associated the risk of dissection could not be assessed. Further research should address the relationship between vessel diameter, vessel composition, vessel wall tension, and SCAD development.

5. Conclusion

Complex vascular anatomy and local flow disturbances were analytically described in coronary artery segments site of a SCAD after complete healing. The finding of a clear prevalence of high local values of vessel curvature and/or torsion in regions where the dissection was hypothesized to have originated suggested a pathophysiologic interaction. Bifurcation site of dissection presented a milder co-localization with local curvature/torsion peak values. Non-partitioning tortuous vascular segments site of SCAD showed markedly deranged shear forces, with high-magnitude WSS and high variability in the WSS contraction/expansion action along the cardiac cycle, potentially able to affect endothelium continuity. Hence, these results strongly support the hypothesis of a strong interaction between vessel anatomy and shear forces in the pathophysiology of SCAD.

Statement of authorship

AC, MLR, DG, BES, CC, UM and CT provided substantial contributions to the conception of the work, to the analysis and interpretation of data for the work. VS and MW provided substantial contributions to the acquisition of data for the work. RAM, JS, TG, AG and FR provided final approval of the version to be published. All authors take responsibility for all aspects of the reliability and freedom from bias of the data presented and their discussed interpretation.

Acknowledgement of grant support

The InterSCAD registry was supported by the Iten-Kohaut Foundation and the Swiss Heart Foundation. The funding sources were not involved in design and conduction of the present study. MLR, CC, DG and UM have been supported by MIUR FISR—FISR2019_03221 CECOMES.

Conflict of interest

AC has consultancy agreements with Medyria, HiD-Imaging and Nanoflex. JS is supported by a Monash University scholarship and received speaker's fees from Abbott and Edwards Lifesciences and a travel grant from Abbott. BS received research grants to the institution from the OPO Foundation, the Iten-Kohaut Foundation, the German Center for Cardiovascular Research (DZHK), Boston Scientific, and Edwards Lifesciences and has received consulting and speaker fees from Boston Scientific and Abbott Vascular. CT received institutional grants from Abbott Vascular, Medtronic, SMT, the Iten-Kohaut Foundation and the Swiss Heart Foundation as well as consulting grants from Biotronik, Microport, Schnell Medical. CT and BS have been supported by the H.H. Sheikh Khalifa bin Hamad Al-Thani Research Programme. The remaining authors have nothing to disclose.

Acknowledgments

None.

Appendix A. Supplementary data

Supplementary data to this article can be found online at https://doi.org/10.1016/j.ijcard.2023.05.006.

References

[1] F. Alfonso, M. Paulo, N. Gonzalo, J. Dutary, P. Jimenez-Quevedo, V. Lennie, J. Escaned, C. Banuelos, R. Hernandez, C. Macaya, Diagnosis of spontaneous coronary artery dissection by optical coherence tomography, J. Am. Coll. Cardiol. 59 (12) (2012) 1073–1079.

[2] R. Mori, F. Macaya, F. Giacobbe, P. Salinas, M. Pavani, A. Boi, L. Bettari, C. Rolfo, I. Porto, N. Gonzalo, F. Varbella, E. Cerrato, J. Escaned, Clinical outcomes by angiographic type of spontaneous coronary artery dissection, EuroIntervention 17 (6) (2021) 516–524.

[3] D. Adlam, F. Alfonso, A. Maas, C. Vrints, C. Writing, European Society of Cardiology, acute cardiovascular care association, SCAD study group: a position paper on spontaneous coronary artery dissection, Eur. Heart J. 39 (36) (2018) 3353–3368.

[4] F. Macaya, P. Salinas, N. Gonzalo, A. Fernandez-Ortiz, C. Macaya, J. Escaned, Spontaneous coronary artery dissection: contemporary aspects of diagnosis and patient management, Open Heart 5 (2) (2018), e000884.

[5] M.F. Eleid, R.R. Guddeti, M.S. Tweet, A. Lerman, M. Singh, P.J. Best, T.J. Vrtiska, M. Prasad, C.S. Rihal, S.N. Hayes, R. Gulati, Coronary artery tortuosity in spontaneous coronary artery dissection: angiographic characteristics and clinical implications, Circ. Cardiovasc. Interv. 7 (5) (2014) 656–662.

[6] U. Morbiducci, A.M. Kok, B.R. Kwak, P.H. Stone, D.A. Steinman, J.J. Wentzel, Atherosclerosis at arterial bifurcations: evidence for the role of haemodynamics and geometry, Thromb. Haemost. 115 (3) (2016) 484–492.

[7] F. Gijsen, Y. Katagiri, P. Barlis, C. Bourantas, C. Collet, U. Coskun, J. Daemen, J. Dijkstra, E. Edelman, P. Evans, K. van der Heiden, R. Hose, B.K. Koo, R. Krams, A. Marsden, F. Migliavacca, Y. Onuma, A. Ooi, E. Poon, H. Samady, P. Stone, K. Takahashi, D. Tang, V. Thondapu, E. Tenekecioglu, L. Timmins, R. Torii, J. Wentzel, P. Serruys, Expert recommendations on the assessment of wall shear stress in human coronary arteries: existing methodologies, technical considerations, and clinical applications, Eur. Heart J. 40 (41) (2019) 3421–3433.

[8] A. Candreva, G.D. Nisco, M.L. Rizzini, F. D'Ascenzo, G.M.D. Ferrari, D. Gallo, U. Morbiducci, C. Chiastra, Current and future applications of computational fluid dynamics in coronary artery disease, Rev. Cardiovasc. Med. 23 (11) (2022).

[9] A. Kumar, E.W. Thompson, A. Lefieux, D.S. Molony, E.L. Davis, N. Chand, S. Fournier, H.S. Lee, J. Suh, K. Sato, Y.A. Ko, D. Molloy, K. Chandran, H. Hosseini, S. Gupta, A. Milkas, B. Gogas, H.J. Chang, J.K. Min, W.F. Fearon, A. Veneziani, D. P. Giddens, S.B. King 3rd, B. De Bruyne, H. Samady, High coronary shear stress in patients with coronary artery disease predicts myocardial infarction, J. Am. Coll. Cardiol. 72 (16) (2018) 1926–1935.

[10] V. Tufaro, H. Safi, R. Torii, B.K. Koo, P. Kitslaar, A. Ramasamy, A. Mathur, D. A. Jones, R. Bajaj, E. Erdogan, A. Lansky, J. Zhang, K. Konstantinou, C.D. Little, R. Rakhit, G.V. Karamasis, A. Baumbach, C.V. Bourantas, Wall shear stress estimated by 3D-QCA can predict cardiovascular events in lesions with borderline negative fractional flow reserve, Atherosclerosis 322 (2021) 24–30.

[11] A. Candreva, M. Pagnoni, M.L. Rizzini, T. Mizukami, E. Gallinoro, V. Mazzi, D. Gallo, D. Meier, T. Shinke, J.P. Aben, S. Nagumo, J. Sonck, D. Munhoz, S. Fournier, E. Barbato, W. Heggermont, S. Cook, C. Chiastra, U. Morbiducci, B. De Bruyne, O. Muller, C. Collet, Risk of myocardial infarction based on endothelial shear stress analysis using coronary angiography, Atherosclerosis 342 (2022) 28–35.

[12] M. Lodi Rizzini, D. Gallo, G. De Nisco, F. D'Ascenzo, C. Chiastra, P.P. Bocchino, F. Piroli, G.M. De Ferrari, U. Morbiducci, Does the inflow velocity profile influence physiologically relevant flow patterns in computational hemodynamic models of left anterior descending coronary artery? Med. Eng. Phys. 82 (2020) 58–69.

[13] L.M. Sangalli, P. Secchi, S. Vantini, A. Veneziani, Efficient estimation of three-dimensional curves and their derivatives by free-knot regression splines, applied to the analysis of inner carotid artery centrelines, J. R. Stat. Soc. 58 (3) (2009) 285–306. Series C (Applied Statistics).

[14] D. Gallo, O. Vardoulis, P. Monney, D. Piccini, P. Antiochos, J. Schwitter, N. Stergiopulos, U. Morbiducci, Cardiovascular morphometry with high-resolution 3D magnetic resonance: first application to left ventricle diastolic dysfunction, Med. Eng. Phys. 47 (2017) 64–71.

[15] D. Gallo, D.A. Steinman, U. Morbiducci, An insight into the mechanistic role of the common carotid artery on the hemodynamics at the carotid bifurcation, Ann. Biomed. Eng. 43 (1) (2015) 68–81.

[16] P. Tasso, A. Raptis, M. Matsagkas, M.L. Rizzini, D. Gallo, M. Xenos, U. Morbiducci, Abdominal aortic aneurysm endovascular repair: profiling postimplantation morphometry and hemodynamics with image-based computational fluid dynamics, J. Biomech. Eng. 140 (11) (2018).

[17] U. Morbiducci, V. Mazzi, M. Domanin, G. De Nisco, C. Vergara, D.A. Steinman, D. Gallo, Wall shear stress topological skeleton independently predicts long-term restenosis after carotid bifurcation endarterectomy, Ann. Biomed. Eng. 48 (12) (2020) 2936–2949.

[18] V. Mazzi, D. Gallo, K. Calo, M. Najafi, M.O. Khan, G. De Nisco, D.A. Steinman, U. Morbiducci, A Eulerian method to analyze wall shear stress fixed points and manifolds in cardiovascular flows, Biomech. Model. Mechanobiol. 19 (5) (2020) 1403–1423.

[19] S. Ciurica, M. Lopez-Sublet, B.L. Loeys, I. Radhouani, N. Natarajan, M. Vikkula, A. Maas, D. Adlam, A. Persu, Arterial tortuosity, Hypertension 73 (5) (2019) 951–960.

[20] D.Y. Li, B. Brooke, E.C. Davis, R.P. Mecham, L.K. Sorensen, B.B. Boak, E. Eichwald, M.T. Keating, Elastin is an essential determinant of arterial morphogenesis, Nature 393 (6682) (1998) 276–280.

[21] P.B. Dobrin, T.H. Schwarcz, W.H. Baker, Mechanisms of arterial and aneurysmal tortuosity, Surgery 104 (3) (1988) 568–571.

[22] E.S. Zegers, B.T. Meursing, E.B. Zegers, A.J. Oude Ophuis, Coronary tortuosity: a long and winding road, Neth. Hear. J. 15 (5) (2007) 191–195.

[23] V. Kunadian, A. Chieffo, P.G. Camici, C. Berry, J. Escaned, A. Maas, E. Prescott, N. Karam, Y. Appelman, C. Fraccaro, G.L. Buchanan, S. Manzo-Silberman, R. Al-Lamee, E. Regar, A. Lansky, J.D. Abbott, L. Badimon, D.J. Duncker, R. Mehran, D. Capodanno, A. Baumbach, An EAPCI expert consensus document on ischaemia with non-obstructive coronary arteries in collaboration with European Society of Cardiology Working Group on coronary pathophysiology & microcirculation endorsed by coronary vasomotor disorders international study group, EuroIntervention 16 (13) (2021) 1049–1069.

[24] P.J. Barbour, J.E. Castaldo, A.D. Rae-Grant, W. Gee, J.F. Reed 3rd, D. Jenny, J. Longennecker, Internal carotid artery redundancy is significantly associated with dissection, Stroke 25 (6) (1994) 1201–1206.

[25] C. Di Donna, A.U. Cavallo, L. Pugliese, F. Ricci, V. De Stasio, M. Presicce, L. Spiritigliozzi, F. Di Tosto, M. Di Luozzo, S. Muscoli, L. Benelli, F. D'Errico, M. Pasqualetto, F.P. Sbordone, F. Grimaldi, V. Meschini, R. Verzicco, F. Romeo, R. Floris, M. Chiocchi, Anatomic features in SCAD assessed by CCT: a propensity score matching case control study, Ann. Cardiol. Angeiol. (Paris) 70 (3) (2021) 161–167.

[26] B. Melchior, J.A. Frangos, Shear-induced endothelial cell-cell junction inclination, Am. J. Phys. Cell Phys. 299 (3) (2010) C621–C629.

[27] V. Mazzi, G. De Nisco, A. Hoogendoorn, K. Calo, C. Chiastra, D. Gallo, D. A. Steinman, J.J. Wentzel, U. Morbiducci, Early atherosclerotic changes in coronary arteries are associated with endothelium shear stress contraction/expansion variability, Ann. Biomed. Eng. 49 (9) (2021) 2606–2621.

[28] T.M. Waterbury, M.S. Tweet, S.N. Hayes, M.F. Eleid, M.R. Bell, A. Lerman, M. Singh, P.J.M. Best, B.R. Lewis, C.S. Rihal, B.J. Gersh, R. Gulati, Early natural history of spontaneous coronary artery dissection, Circ. Cardiovasc. Interv. 11 (9) (2018), e006772.

[29] M. Lodi Rizzini, A. Candreva, C. Chiastra, E. Gallinoro, K. Calo, F. D'Ascenzo, B. De Bruyne, T. Mizukami, C. Collet, D. Gallo, U. Morbiducci, Modelling coronary flows: impact of differently measured inflow boundary conditions on vessel-specific computational hemodynamic profiles, Comput. Methods Prog. Biomed. 221 (2022), 106882.